# Thin Polymer Films from Fluidized Electrode Bed Reactors

F. S. TENG and R. MAHALINGAM,* *Department of Chemical Engineering, Washington State University, Pullman, Washington 99164-2710*

## Synopsis

The formation and deposition of a polymer as a thin, uniform solid film on a metal particle substrate is investigated in detail in a fluidized electrode bed reactor. Experiments were carried out in different designs of fluidized bed electrode cell reactor, using various metal particles and monomers. It was observed that diacetone acrylamide (DAA) monomer in 0.1$N$ $H_2SO_4$ with aluminum particles (3530 $\mu$m) as cathode, in a concentric dual compartment cell, appeared to yield the best films. Infrared and elemental analyses were used to characterize the polymer film on the metal particles. Scanning electron microscopy (SEM) was employed to examine the surface and cross-sectional profiles of the films. The potential profiles in both particulate and solution phases were measured and the importance of particulate electrical conductivity in the polymerization is thus explained. It was observed that the optimum particulate conductivity and hence the maximum yield occurs in the range of 10–20% bed expansion. The experimental product yields for various liquid superficial velocities (i.e., bed expansion) at different feeder current densities were compared to explain the possible controlling mechanism in packed and fluidized bed cells, noting that both chemical reaction and mass transfer control in the low bed expansion region while chemical reaction controls in the high bed expansion region. The current efficiency decreases in the high current region due to side reactions at the fluidized bed electrode and due to pore diffusion in the polymer film.

## INTRODUCTION

The successful application of electroinitiated polymerization for formation of films on cathodic metal surfaces in batch reactors has previously been reported by Teng et al.[1] The polymer yield on the cathode is found to be a function of current density, time, concentration of monomer, electrode materials, electrolyte, etc. This work has been extended by Mahalingam et al.[2] to fluidized electrode bed reactors, with the objective of forming polymeric films on metallic and metal-coated nonmetallic particulate substrates. In such a system, metal particles form the cathode, thus making available low current densities because of a large electrode surface area per unit volume of the bed. Furthermore, the continuous disturbance of the bed contributes to the preferred high rates of mass transfer to the surface of the particles. Polymer films developed though this technique and process have recently become technically and commercially important in view of their potential applications in the preparation of advanced technology materials such as composites, solar collectors, electrooptical sensors and devices, and separation membranes.

*To whom correspondence should be addressed.

Journal of Applied Polymer Science, Vol. 34, 2837–2852 (1987)
 CCC 0021-8995/87/082837-16$04.00

## BACKGROUND

In electropolymerization reactions, the electrode process is the source of active species that initiates polymerization, in the solution and/or at the electrode.[3] Albeck et al.[4] studied the electroinitiated polymerization of acrylates and methacrylates in methanol solution containing lithium acetate as electrolyte, and suggested a free-radical mechanism. Bruno et al.[5] and Pham et al.[6] obtained thin films of reactive polymers on metal surfaces by electrochemical polymerization of disubstituted phenols. Such thin film development on electrodes has been reviewed by Subramanian.[7] More recent work has been aimed at forming conductive polymer films on metals[8,9] or on electrode surface modification through polymer films carrying desirable functional groups.[10]

## EXPERIMENTAL

**Materials.** Acrylonitrile (AN) (Aldrich) was freed of hydroquinone inhibitor by washing with 5% NaOH and then with 5% $H_3PO_4$, followed by drying under anhydrous $CaSO_4$ for several days and finally by distillation under reduced pressure. Acrylic acid (AA), (Aldrich) was distilled under reduced pressure and the middle fraction used. Diacetone Acrylamide (DAA) (Polysciences, Inc.) and concentrated $H_2SO_4$ (Mallinckrodt, analytical grade) were used without additional treatment. Aluminum shots (417–509 $\mu$m) and s-steel shots (417–590 $\mu$m) were obtained from Pellets, Inc., New York. Aluminum cylindrical particles (1/8 × 1/8 in.) were obtained by cutting aluminum rods (1/8 in. diameter, 94% Al and 5% Si) (Gibson Co., Spokane, WA). The equivalent particle diameter $d_p$ and sphericity factor $s$ of the aluminum cylindrical particles were calculated as 0.353 cm and 0.870, respectively. The particles were first washed with distilled water, next with acetone, and then degreased with trichloroethylene, prior to the polymerization runs.

**Electrode Bed Reactor.** The dual compartment cell with concentric configuration was fabricated from a polysulfone rod (3 in. diameter and 12 in. long) (Fig. 1). The space was divided into outside anode and inside cathode compartments by a cylindrical alundum thimble (1.7 in. O.D. × 4.0 in. long, Scientific Products), glued to the upper part of the cell. A removable perforated Teflon plate was positioned between the upper and lower parts held tight by a clamp. In the case of aluminum particles, an aluminum feeder electrode (1/8 in. diameter) was inserted into the bed in the cathode chamber; surrounding the alundum thimble was a cylindrical counter electrode of platinum (2 in. diameter × 2 in. long). Power for the cell was obtained from a direct current power supply unit (Trygon RS) capable of delivering either voltage or current, controlled up to 350 V or 2 A, respectively. A two-channel chart recorder (Hewlett-Packard, 7128A) in series with the circuit and connected with a 10 Ω shunt resistor continuously monitored the cell current and recorded the potential profile in the fluidized bed reactor. The flow circulation diagram is shown in Figure 2. A dual flow recirculation system was used during the electropolymerization. A monomer or comonomer solution containing 0.1$N$ $H_2SO_4$ was pumped through the cathode compartment, while the $H_2SO_4$ electrolyte solution, without any monomer in it, was circulated through the anode compartment. Both the catholyte and anolyte were cooled through

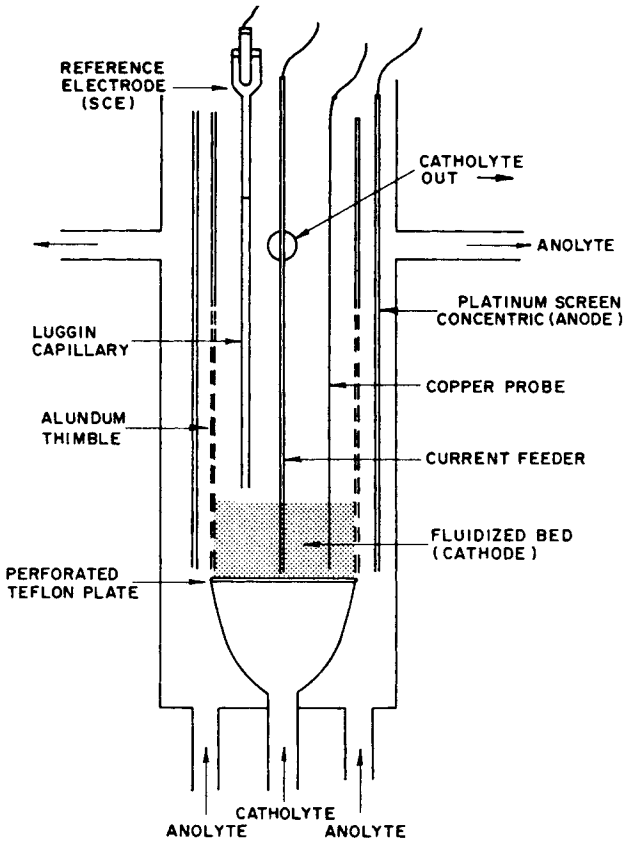


Fig. 1. Dual-compartment fluidized electrode bed reactor, concentric configuration.

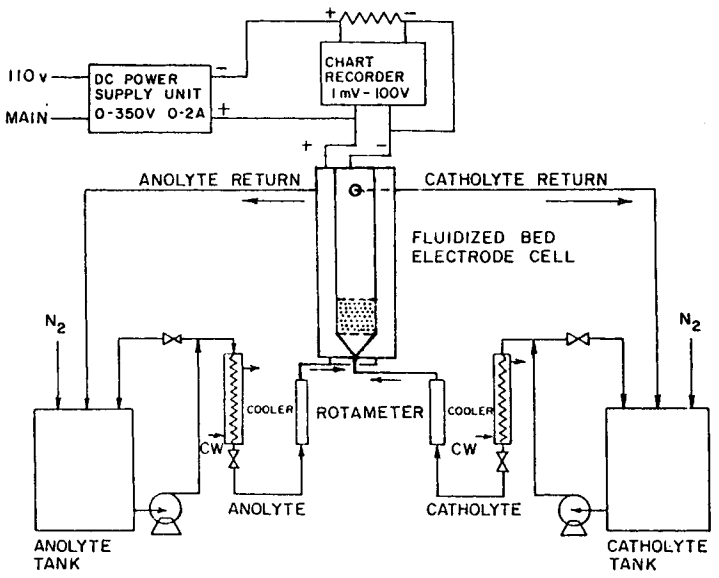


Fig. 2. Flow setup for electropolymerization in fluidized electrode bed reactor.

water-cooled heat exchangers. After a polymerization run time of 90 min, the amount of polymer film deposited on the metal particles was determined by weight difference.

The radial variation of potentials in the particulate and solution phases was monitored by two electrode probes which were inserted, as necessary, into the cathode compartment. The potential profile in the particulate phase was measured with a copper sphere of diameter about 0.1 cm attached to the tip of a copper wire, insulated by a thermally shrunk plastic tube. The Luggin capillary whose tip was positioned right above the particulate phase connected to a standard calomel electrode (SCE) monitored the solution potential. The two probe electrodes traversed the bed cell over equal spacings between the current feeder and the internal wall of the diaphragm. Potential drops with respect to the current feeder were recorded on the chart.

**Analyses.** A Perkin-Elmer Model 700 IR spectrophotometer was used to establish the polymer functional groups. Elemental analyses of the polymer film was carried out on a Perkin-Elmer Model 240 elemental analyzer. Neutron activation analyses on the metals were carried out by simultaneous irradiation of a standard sample, 5 min for Al and 8 h for stainless steel, at the WSU TRIGA Nuclear reactor. Activities were measured with a Ge(Li) detector. The polymer films were observed under the SEM, TEC Auto Scan model, after sputter coating with gold.

## RESULTS AND DISCUSSION

**SEM Examination of Polymer Films.** The film surface and cross-sectional structure were examined under the SEM. For purposes of comparison, bare metal, metal oxide and polymer coating surfaces are shown in Figures 3(a–d). It can be seen in Figure 3(b), at the higher magnification, that some metal oxide was usually present on the bare aluminum surface; under both magnifications, the polymer film could be seen formed on the aluminum particle, this corresponding to a run wherein the monomer used was a 0.5*M* DAA in 0.1*N* $H_2SO_4$ solution. The cross-sectional profile of PDAA coatings obtained on the above aluminum particles is shown in Figure 3(e). The thickness of the coating could be seen to be approximately 7 $\mu$m. The film on s-steel particles, under two magnifications, are shown in Figures 4(a–d). Here, the catholyte used was a 120 mL monomer mixture (50%AN and 50%AA) in 1200 mL 0.1*N* $H_2SO_4$ solution. Comparison of SEM pictures in Figures 3 and 4 show the copolymer film on the s-steel particles to be rough, porous, and nonuniform while the PDAA film on the aluminum surface was more uniform and quite thick. It should be recalled that there was observed to be metal oxide present in both PDAA and poly(AN–CO–AA) films obtained on aluminum and s-steel plate surfaces.[1,2]

**Bed Characteristics.** Prior to the actual electropolymerization in the packed and fluidized bed electrode cells, different metal particles were used to study the relationship between liquid superficial velocity and bed porosity in the fluidized bed. The catholyte superficial velocity was monitored and for each but different liquid superficial velocity $V$, the corresponding expanded bed height $H$ was measured. The bed porosity was then determined. A logarithmic plot of bed porosity $\epsilon$ vs. liquid superficial velocity $V$, with

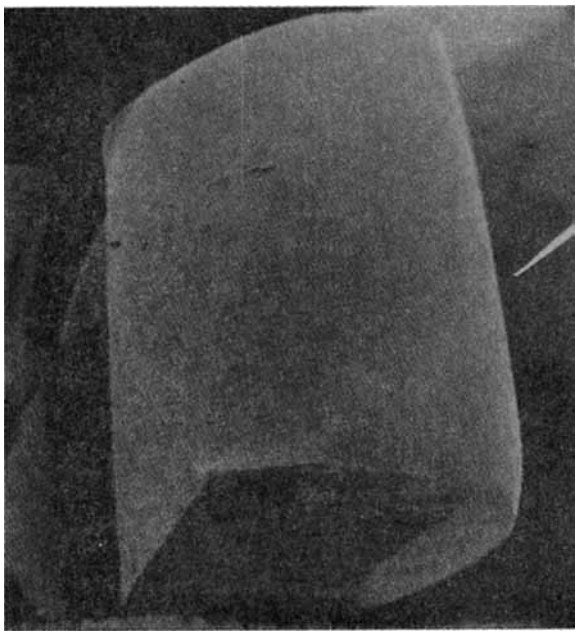

(a)

(b)

Fig. 3. Scanning electron micrographs of uncoated aluminum particle and aluminum particle coated with PDAA in fluidized bed cell; concentric configuration: (a) surface structure of uncoated aluminum particle of equivalent diameter 3530 $\mu$m, at 20 $\times$ ; (b) surface structure of uncoated aluminum particle of equivalent diameter 3530 $\mu$m, at 1000 $\times$ ; (c) surface structure of PDAA on aluminum particle of equivalent diameter 3530 $\mu$m, at 20 $\times$ ; (d) surface structure of PDAA on aluminum particle of equivalent diameter 3530 $\mu$m, at 1000 $\times$ ; (e) cross-sectional profile, at 1000 $\times$ , of PDAA film on aluminum particle of equivalent diameter 3530 $\mu$m.

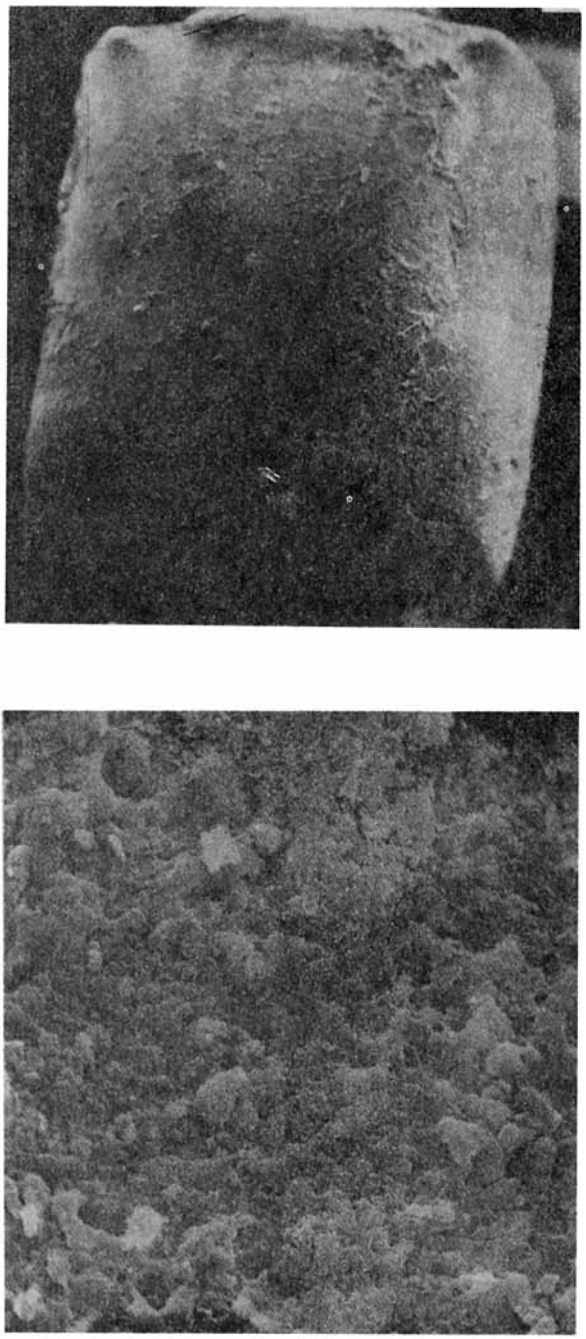

(d)

Fig. 3. (*Continued from the previous page.*)

(c)

Fig. 3. (*Continued from the previous page.*)

aluminum particles as the particulate phase, is shown in Figure 5. The bed porosity is ~ 0.61 at a minimum fluidization velocity $V_{MF}$ of 2 cm/s. Next, an attempt was made to correlate the bed porosity through established relationships.[11] The Ergun equation can be written as

$$\frac{1.75\mathrm{Re}^2}{S\epsilon^3} + \frac{150\mathrm{Re}(1-\epsilon)}{S^2\epsilon^3} - C = 0 \tag{1}$$

where $C$ is independent of the flow rate and bed porosity. The two limiting cases of the Ergun equation are the Blake–Plummer equation which holds for large particle Reynolds numbers with velocity $V$ proportional to $\epsilon^{3/2}$ and the Kozeny–Carman equation which holds for low particle Reynolds numbers with velocity $V$ proportional to $\epsilon^3/(1-\epsilon)$. As shown in Figure 6, the liquid velocity is plotted versus both $\epsilon^{3/2}$ and $\epsilon^3/(1-\epsilon)$. It was found that the relationship between liquid superficial velocity and bed porosity is consistent with the Kozeny–Carman equation in the low Reynolds number region and the Blake–Plummer equation in the high Reynolds number region. The transition region between the above two cases occurred at a particle Reynolds number of about 85. The bed characteristics will be related to the polymer yield in a later section.

**Potential Profiles.** As described earlier, the solution and particulate potentials were both measured with respect to the current feeder, the former against a saturated calomel electrode (SCE) and the latter directly, for various bed expansions, and are shown in Figure 7. Here the $y$-axis values are in terms of the absolute values of the potentials; thus the experimental values of the

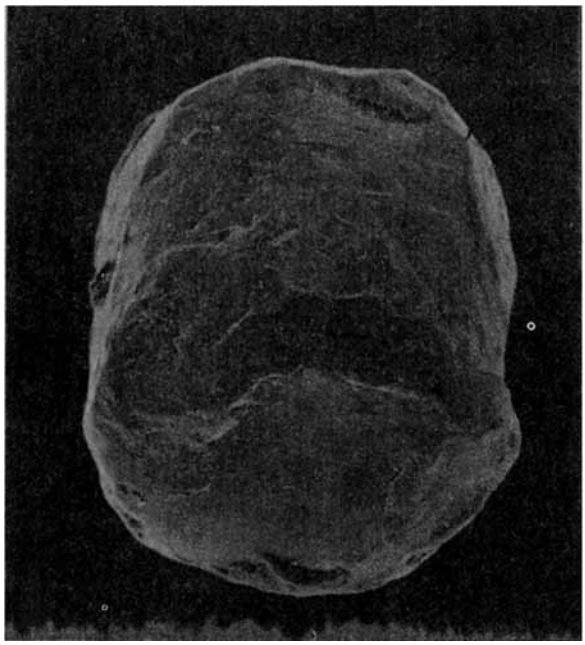

(a)

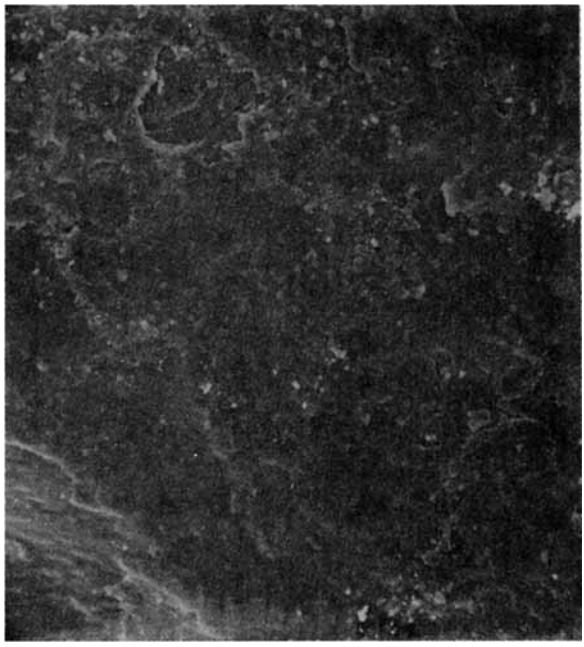

(b)

Fig. 4. Surface structure, under SEM, of uncoated s-steel particle and s-steel particle coated with poly(AN–CO–AA) in fluidized bed cell (concentric configuration): (a) uncoated s-steel particle of ~ 500 $\mu$m at 100 ×; (b) uncoated s-steel particle of ~ 500 $\mu$m at 1000 ×; (c) poly(AN–CO–AA) on s-steel particle of ~ 500 $\mu$m at 100 ×; (d) poly(AN–CO–AA) on s-steel particle of ~ 500 $\mu$m at 1000 ×.

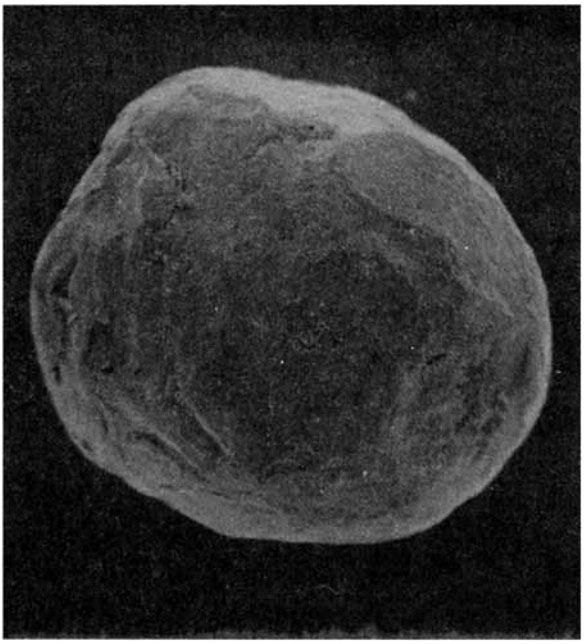

(c)

(d)

Fig. 4. (*Continued from the previous page.*)

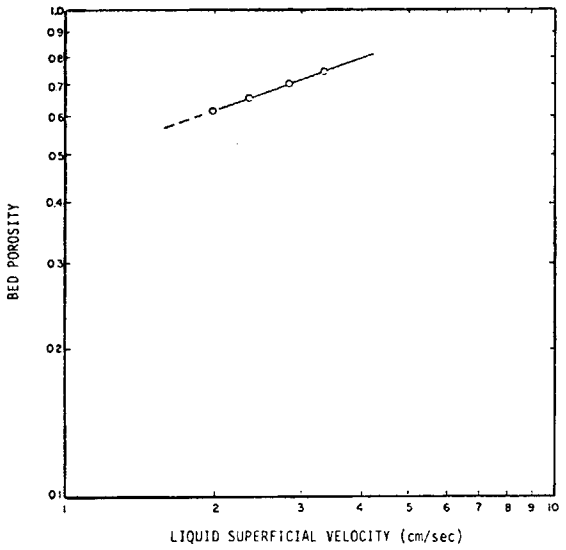


Fig. 5. Bed porosity vs. liquid superficial velocity for fluidized bed cell: (0)Al particles (3530 $\mu$m).

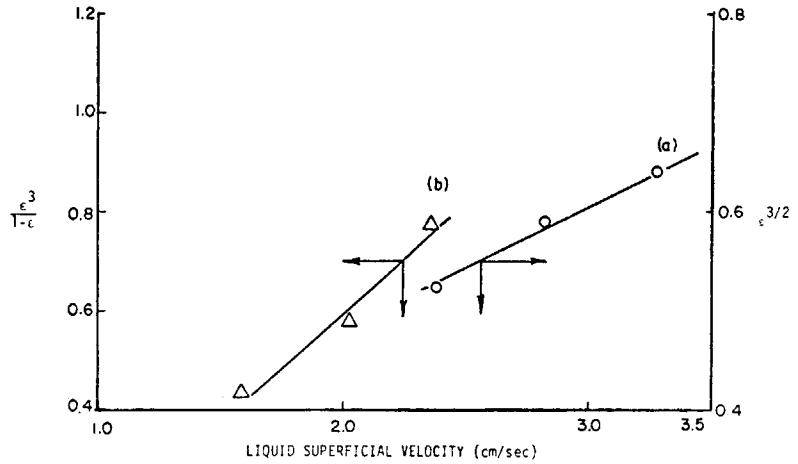


Fig. 6. Porosity vs. liquid superficial velocity for concentric configuration: (a) $\epsilon^{3/2}$ vs. $V$; (b) $\epsilon^3/1 - \epsilon$ vs. $V$.

potential presented are after correcting the measured values for the SCE voltage (0.24 V). The catholyte for these runs was a 0.5$M$ DAA in 0.1$N$ $H_2SO_4$ solution and the anolyte was monomer-free aqueous 0.1$N$ $H_2SO_4$; the feeder current density was maintained at 10 mA/cm$^2$ for 90 min. It was found that potential drops in both the particulate and solution phases increased with distance from the current feeder which was in compliance with Ohm's law. The variation in profiles could be attributed to differing controlling mechanisms in the different bed expansion regions. This will also be related to polymer yield, in a later section.

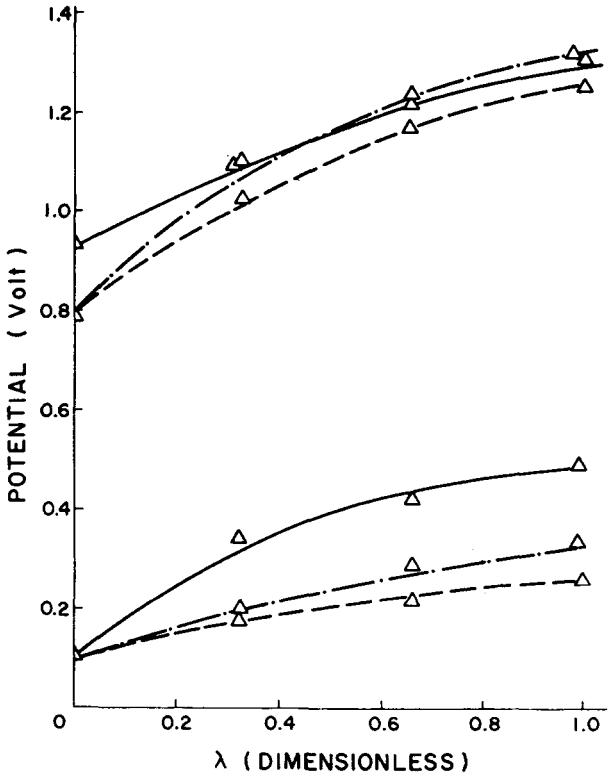


Fig. 7. Radial potential profiles for solution $\phi_s$ (top) and particulate $\phi_p$ (bottom) phases; feeder current density 10 mA/cm$^2$: (—) 35% bed expansion; (— · —) incipient fluidization; (– – –) 10% bed expansion.

**Bed Conductivity vs. Bed Expansion.** The effect of bed expansion on the electrical conductivity in the particulate phase, for current density parameter, is shown in Figures 8(a–c). It was found that the potential drop in the particulate phase at any radial location decreased with increasing flow velocity (increasing bed expansion) in the low flow velocity region, i.e., the electrical conductivity increased. This increase can be explained in terms of the polarization curves of a pseudocurrent density vs. cathode potential which have been developed during the authors' preliminary studies[2] on fluidized bed system (side-by-side configuration) with smaller aluminum particles (417–590 $\mu$m), in 0.5$M$ DAA, 0.1$N$ $H_2SO_4$ solution. In the high flow velocity region, the potential drop in the particulate phase increased with bed expansion, i.e., the electrical conductivity in the particulate phase decreased. This is explained on the basis of poor contact between individual metal particles at higher bed expansion.

The optimum electrical conductivity in the particulate phase is thus seen to occur in the range of 10–20% bed expansion. Goodridge et al.[12] in their cathodic reduction of *m*-nitrobenzene sulfonic acid to metanilic acid in the fluidized bed electrode, with sulfuric acid as electrolyte, did point out the importance of bed expansion in establishing the best particulate conductivity and the maximum operating performance for a fluidized bed electrode. They

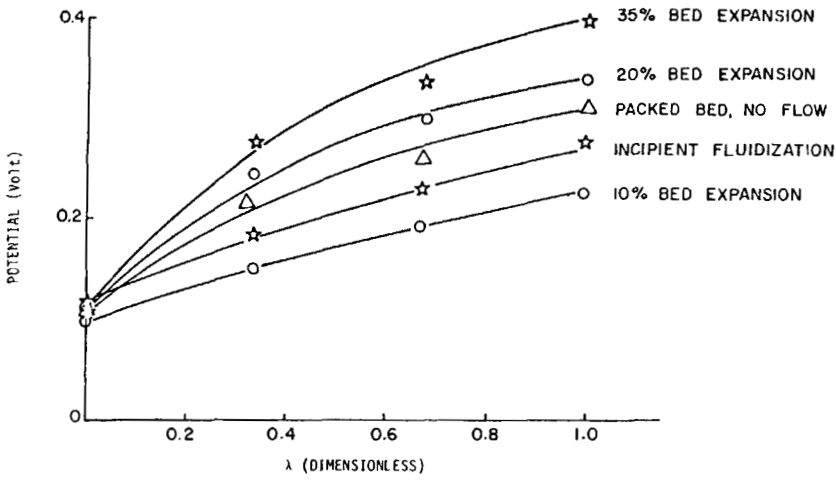


(a)

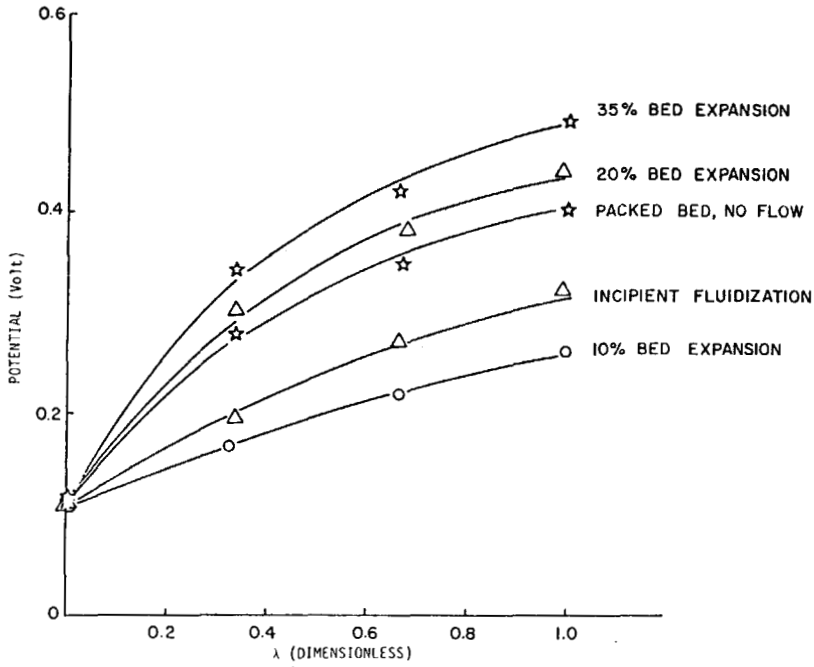


(b)

Fig. 8. Dependence of potential drop in particulate phase on bed expansion at different feeder current densities (mA/cm$^2$): (a) 6.7; (b) 10; (c) 16.7.

indicated that the optimum bed expansion is 5–25%, comparable to 10–20% in our experiments.

**Polymerization Reaction Rates.** As mentioned earlier, the experimental electropolymerization rate was calculated by the weight increase of polymer on aluminum particles. The results were compared in terms of dimensionless product yields, the reference yield being at incipient fluidization, for 0.5*M*

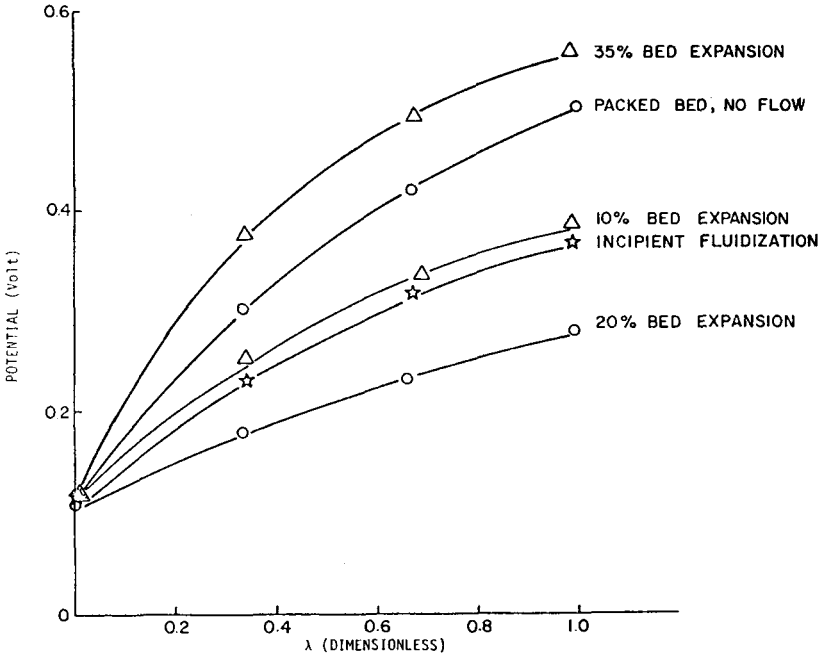


(c)

Fig. 8. *(Continued from the previous page.)*

DAA in 0.1*N* $H_2SO_4$, at 10 mA/cm$^2$ feeder current density. These are plotted in Figure 9. In the low flow velocity (low bed expansion) region, the dimensionless polymer film yield increased rather slowly with bed expansion; as the flow velocity and hence the bed expansion increased furthermore, the film yield decreased rapidly. The maximum yield of polymer film was observed in the range of 10–20% bed expansion.

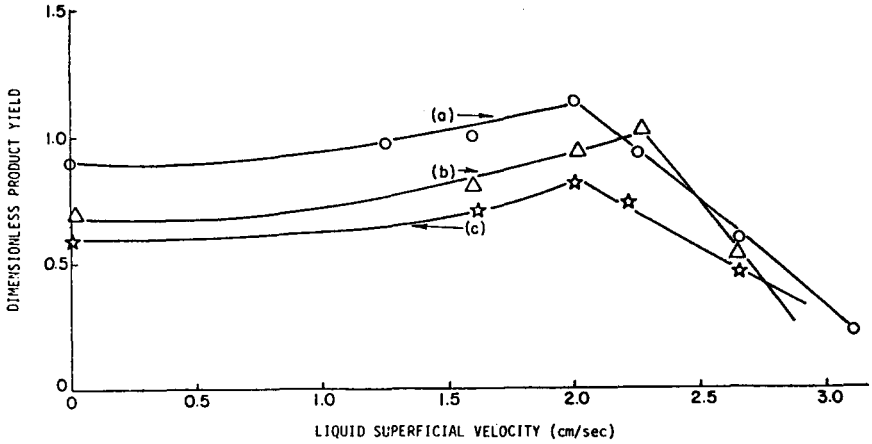


Fig. 9. Effect of flow velocity on polymer film yield at different feeder current densities (mA/cm$^2$) in packed and fluidized bed electrode cells: (a) 10; (b) 16.7; (c) 6.7.

Similar results were observed, as described in the previous section, for particulate conductivity vs. bed expansion, where the highest conductivity was reached in the range of 10–20% bed expansion. This could be explained on the basis that the mass transfer effects were not as important a factor in the high bed expansion regions although chemical reaction was still controlling. Carbin and Gabe[13] studied the optimization of mass transfer in an electrolytic cell containing a fluidized bed of nonconducting particles and explained the agitation in the fluidized bed was primarily due to particle motion and secondarily to the overall fluid flow. Increase in the superficial velocity will cause an increase initially in the mass transfer, but as the bed expands further the specific agitation effect of any individual particle decreases and at high bed porosity the effect of bed expansion in decreasing mass transfer is greater than the effect of flow velocity in increasing mass transfer.[14]

King and Smith,[15] who studied the effect of mass transfer on the reduction of ferricyanide ion in a liquid fluidized bed electrode, found that maximum mass transfer coefficient occurred at a bed porosity of approximately 0.60. The maximum polymer film yield was found to occur at a bed porosity between 0.61 and 0.64 in the present work.

The extent of fluidization also has an effect on the overvoltage for hydrogen evolution. Carbin and Gabe[13] found that the hydrogen overvoltage decreases as the bed expansion increases, i.e., hydrogen is easier to evolve at the metal

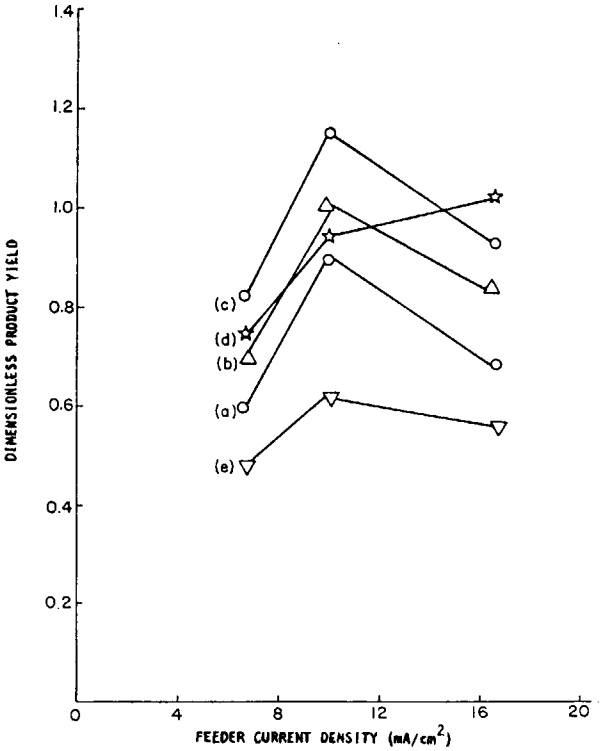


Fig. 10. Effect of feeder current density on polymer film yield in packed and fluidized electrode cells at various bed expansions: (a) packed bed, no flow; (b) incipient fluidization; (c) 10% expansion; (d) 20% expansion; (e) 35% expansion.

particles at high bed expansion, and this increases the difficulty to get a film deposit on the metal particles at high flow velocity; this, in turn, reduces the product yield since the yield is calculated based on the amount adhering to the substrate. It should also be emphasized here that the electrochemical reaction is important for all bed expansion conditions; the electrochemical reduction of hydrogen ion to hydrogen atom has an activation energy of about 1 kcal/g mol[16] whereas the activation energy of electropolymerization, which occurs after the formation of hydrogen atom in our fluidized bed cell, is about 6 kcal/g mol.[17] The rate parameters in polymer film formation through electropolymerization are discussed by Teng and Mahalingam, elsewhere.[18]

The effect of feeder current density on the polymer film yield in the packed and fluidized bed electrodes is shown in Figure 10. It is found that the polymer yield increases with the applied current at the current feeder, goes through a maximum, and then falls off as the current is increased further. These results imply that the efficiency of polymer production is inhibited with increased current density, i.e., current efficiency is reduced at higher current density region. Such an effect has been noted for the previously described stationary cell system.[1] The higher current density leads to a loss of polymer yield due to side reactions and to increased diffusion resistance for current flow through the pores of the film coating.[19]

## APPENDIX: NOMENCLATURE

| | |
|---|---|
| $C$ | constant used in Ergun equation (1) |
| $r$ | radial coordinate in bed |
| $R$ | inner cell radius for dual compartment fluidized bed with concentric configuration |
| Re | particle Reynolds number |
| $s$ | sphericity of cylindrical particles |
| $V$ | liquid superficial velocity |
| $\epsilon$ | bed porosity |
| $\epsilon_{MF}$ | bed porosity at minimum fluidization velocity |
| $\phi_p$, $\phi_s$ | electrical potential in particulate and solution phases |
| $\lambda$ | dimensionless radial coordinate in bed, $r/R$ |

## References

1. F. S. Teng, R. Mahalingam, R. V. Subramanian, and R. A. V. Raff, *J. Electrochem. Soc.*, **124**(7), 995 (1977).
2. R. Mahalingam, F. S. Teng, and R. V. Subramanian, *J. Appl. Polym. Sci.*, **22**, 3587 (1978).
3. B. L. Funt, *Macromol. Rev.*, **1**, 35 (1967).
4. M. Albeck, M. Konigsbuch, and J. Relis, *J. Polym. Sci., A-1*, **9**, 1375 (1971).
5. F. Bruno, M. C. Pham, and J. E. Dubois, *Electrochimica Acta*, **22**, 451 (1977).
6. M. C. Pham, P. C. Lacaze, and J. E. Dubois, *J. Electroanall. Chem.*, **86**, 147 (1978).
7. R. V. Subramanian, *Adv. Polym. Sci.*, **33**, 34 (1979).
8. J. Bargon, S. Mohmand, and R. S. Waltman, *IBM J. Res. Dev.*, **27**, 330 (1983).
9. I. Rubinstein, *J. Polym. Sci., Polym. Chem. Ed.*, **21**, 3035 (1983).
10. R. W. Murray, in *Electroanalytical Chemistry*, A. J. Bard, Ed., Dekker, New York, 1984, Vol. 13.

11. S. Ergun, *Chem. Eng. Prog.*, **48**, 89 (1952).
12. F. Goodridge, D. I. Holden, H. D. Murray, and R. E. Plimley, *Trans. Inst. Chem. Eng.*, **49**, 128 (1971).
13. D. C. Carbin, and D. R. Gabe, *Electrochimica Acta*, **19**, 645 (1974).
14. G. H. Sedahmed, *Can. J. Chem. Eng.*, **64**(2), 75 (1986).
15. D. H. King, and J. W. Smith, *Can. J. Chem. Eng.*, **45**, 329 (1967).
16. R. H. Perry and C. H. Chilton, *Chemical Engineers' Handbook*, 5th ed., McGraw-Hill, New York, 1973, pp. 4–37.
17. F. W. Billmeyer, Jr., *Textbook of Polymer Science*, 2nd ed., Wiley, New York, 1970.
18. F. S. Teng, and R. Mahalingam, *Polym. Commun.*, **27**(11), 342 (1986).
19. Ya. D. Zytner, and K. A. Makarov, *Polym. Sci. USSR*, **22**(11), 2866 (1980).

Received February 27, 1987
Accepted April 15, 1987